Isotopically "heavy" pyrite in marine sediments due to high sedimentation rates and non-steady-state deposition

Isotopically 'heavy' pyrite in marine sediments due to high sedimentation rates and non-steady-state deposition

Jiarui Liu[1,2*], Gilad Antler[3,4], André Pellerin[1,3], Gareth Izon[5],

Ingrid Dohrmann[6], Alyssa J. Findlay[1], Hans Røy[1], Shuhei Ono[5],

Alexandra V. Turchyn[7], Sabine Kasten[6,8], and Bo Barker Jørgensen[1]

[1]Section for Microbiology, Department of Biology, Aarhus University, 8000 Aarhus C, Denmark

[2]Department of Earth, Planetary and Space Sciences, University of California, Los Angeles, CA 90095, USA

[3]Department of Earth and Environmental Sciences, Ben-Gurion University of the Negev, Beersheba 84105, Israel

[4]The Interuniversity Institute for Marine Sciences, Eilat 88103, Israel

[5]Department of Earth, Atmospheric and Planetary Sciences, Massachusetts Institute of Technology, Cambridge, MA 02139, USA

[6]Alfred Wegener Institute Helmholtz Centre for Polar and Marine Research, 27570 Bremerhaven, Germany

[7]Department of Earth Sciences, University of Cambridge, Cambridge CB2 3EQ, UK

[8]Faculty of Geosciences, University of Bremen, 28359 Bremen, Germany

[*]E-mail: jiaruiliu@ucla.edu.

ABSTRACT

Sedimentary pyrite formation links the global biogeochemical cycles of carbon, sulfur and iron that, in turn, modulate the redox state of the planet's surficial environment over geological timescales. Accordingly, the sulfur isotopic composition ($\delta^{34}S$) of pyrite has been widely employed as a geochemical tool to probe the evolution of ocean chemistry. Characteristics of the depositional environment and post-depositional processes, however, can modify the $\delta^{34}S$ signal that is captured in sedimentary pyrite and ultimately preserved in the geological record. Exploring sulfur and iron diagenesis within the Bornholm Basin, Baltic Sea, we find that higher sedimentation rates limit the near-surface sulfidization of reactive iron, facilitating its burial and hence subsurface availability of reactive iron for continued and progressively more ^{34}S-enriched sediment-hosted pyrite formation ($\delta^{34}S \approx -5‰$). Using a diagenetic model, we show that the amount of pyrite formed at the sediment–water interface has increased over the last few centuries in response to expansion of water-column hypoxia, which also impacts the sulfur isotopic signature of pyrite at depth. This contribution highlights the critical role of reactive iron in pyrite formation and questions to what degree pyrite $\delta^{34}S$ values truly reflect past global ocean chemistry and biogeochemical processes. This work strengthens our ability to extract local paleoenvironmental information from pyrite $\delta^{34}S$ signatures.

INTRODUCTION

Microbially-mediated marine biogeochemical sulfur cycling has played a fundamental role in regulating the chemistry of Earth's surface, coupling redox reactions with organic carbon and molecular oxygen over Earth History (Canfield and Teske, 1996; Garrels and Lerman, 1981). The various redox transformations of sulfur are often accompanied by isotope fractionation, which may then propagate throughout environmentally-relevant sulfur pools (Canfield, 2001; Jørgensen et al., 2019). Given that sedimentary pyrite represents the dominant marine sulfur sink (Berner, 1984), the sulfur isotopic composition ($\delta^{34}S$) of sedimentary pyrite has been frequently employed to elucidate the evolution of ocean chemistry and to detect changes in Earth's surface environment (Canfield and Teske, 1996; Gill et al., 2011; Hammarlund et al., 2012). Recent studies, however, have elucidated that rather than informing on large-scale changes in global sulfur cycling, pyrite $\delta^{34}S$ records integrate multiple signals and are impacted by local depositional and post-depositional processes, such as changes in sedimentation rate (Fike et al., 2015; Lang et al., 2020; Liu et al., 2019; Pasquier et al., 2017).

Pyrite formation is controlled by the availability of both reduced sulfur species and reactive iron (Berner, 1984; Rickard and Luther, 2007). Ultimately, the $\delta^{34}S$ of pyrite is a function of the $\delta^{34}S$ of reduced sulfur species at the depth of pyrite precipitation (Butler et al., 2004). Higher sedimentation rates reduce the exchange of sulfate between sediment porewater and the overlying water-column, allowing more progressive consumption of the sulfate reservoir that increases the $\delta^{34}S$ of both porewater sulfate and sulfide (Goldhaber and Kaplan, 1975; Wijsman et al., 2001). Numerous models have been developed to link the coupled $\delta^{34}S$ evolution of porewater sulfate and sulfide, exploring how the connectivity between porewaters and the overlying water-column affects the isotopic evolution of the pore-fluids (Chernyavsky and Wortmann, 2007; Jørgensen,

1979). Surprisingly, however, despite its known influence on the efficiency and depth of pyrite formation (März et al., 2008; Riedinger et al., 2005, 2017; Shawar et al., 2018), to date, there has been limited work exploring how diagenesis influences the subsurface availability of reactive iron. Studying pyritization through coupled iron and sulfur diagenesis in dynamic depositional regimes, therefore, remains an important approach to the successful translation of pyrite-derived $\delta^{34}S$ records into useful information regarding the operation of the ancient sulfur cycle. As a first-step, here we test a hypothesized positive relationship between sedimentation rates and reactive iron burial, examining how enhanced subsurface reactive iron availability fuels subsurface pyrite genesis and the ingrowth of sedimentary pyrite with more positive $\delta^{34}S$ values.

STUDY AREA AND METHODOLOGY

Within the Bornholm Basin, Baltic Sea (Fig. 1), the underlying glaciogenic topography induces distinct spatial variability in Holocene sedimentation rates (Hilligsøe et al., 2018). Accordingly, the Bornholm Basin offers the opportunity to explore how spatially variable sedimentation rates impact reactive iron availability in the subsurface and its knock-on effects on pyrite genesis and its sulfur isotope systematics. Here, we present a comprehensive dataset comprising sulfur and iron abundance and multiple sulfur isotope data for marine sediments collected at site BB03 in the Bornholm Basin. Over the past 8500 years, the sedimentation rate at site BB03 (113 cm ka^{-1}) has been much higher than neighboring sites (BB02 and BB05; Table S1), thereby allowing us to evaluate the role of the depositional environment on pyrite-$\delta^{34}S$ values across the basin.

Porewater and sediments were sampled and analyzed using established procedures (see Supplemental Material[1]). Sulfur isotope data are presented in standard δ notation relative to Vienna Canyon Diablo Troilite (VCDT):

$$\delta^{3X}S\ (‰) = ({}^{3X}R_{Sample}/{}^{3X}R_{VCDT} - 1) \times 1000, \quad (1)$$

where ${}^{3X}R = {}^{3X}S/{}^{32}S$ (X = 3 or 4). The minor sulfur isotopic composition is defined as deviation of $\delta^{33}S$ from the ideal mass-dependent relationship and reported in $\Delta^{33}S$ notation (Ono et al., 2006):

$$\Delta^{33}S = \delta^{33}S - 1000 \times [(1 + \delta^{34}S/1000)^{0.515} - 1]. \quad (2)$$

THE ROLE OF SEDIMENTATION RATE IN PYRITE FORMATION

Early diagenesis of iron and sulfur involves the transformation of highly reactive Fe minerals (Fe-(oxyhydr)oxides and Fe-carbonates) to Fe-sulfides (Berner, 1984). In core BB03 the extent of pyritization of the highly reactive Fe pool, expressed as Fe_{py}/Fe_{HR}, varies between 0.5 and 0.7 near the sediment–water interface, increasing toward 0.8 downcore, albeit with much scatter (Fig. 2A). This implies that pyrite precipitation starts soon after deposition and pyrite is slowly accumulating throughout burial. Importantly, a positive relationship between sedimentation rate and reactive Fe abundance is seen at the three sites (Figs. 2C, 3C). Under higher sedimentation rates, the contact time between the sulfidic porewaters and available reactive Fe phases is minimized, promoting the burial and preservation of reactive Fe (März et al., 2008; Riedinger et al., 2005, 2017). At depth, these Fe-oxides can enhance sulfide oxidation and deep S^0 formation down to 450 cmbsf (cm below seafloor), thus pyrite formation can be active throughout the four-thousand-years of deposition at site BB03 (Fig. S1).

Microbial sulfate reduction preferentially consumes ^{32}S over ^{34}S by up to 70‰ (Sim et al., 2011), enriching the residual porewater sulfate in ^{34}S, as seen in the subsequently formed H_2S (Fig.

3A; Canfield, 2001; Pellerin et al., 2018). With this in mind, the ^{34}S-enriched pyrite seen at site BB03 reflects the combined product of early- and late-formed pyrite (Fig. S2), as supported by the multiple sulfur isotope systematics. Masterson (2016) showed that the $\delta^{34}S$ and $\Delta^{33}S$ values of early-formed Baltic Sea pyrite are approximately −30‰ and 0.17‰, respectively, while their late-formed counterparts approximate those of seawater sulfate ($\delta^{34}S$ = 21‰, $\Delta^{33}S$ = 0.05‰; Liu et al., 2020b). The $\delta^{34}S$ and $\Delta^{33}S$ systematics of pyrite extracted from site BB03 lie on the mixing line between these two pyrite pools (Fig. 3B), where mixing results in curved trajectories and progressively lower $\Delta^{33}S$ values (Ono et al., 2006). We also find that the organic matter availability and the connectivity between porewater and overlying water-column do not change with sedimentation rates (Figs. S3–S4). Precluding these variables, we suggest that the more plentiful reactive Fe remains in the subsurface, the more ^{34}S-enriched bulk $\delta^{34}S$ values can become (Figs. 2B–C, 3C–D), providing an explanation for the elevated pyrite-$\delta^{34}S$ values (−5‰) seen below 80 cmbsf at site BB03 (Fig. 2B). Contrastingly, where sedimentation rates are much lower at sites BB02 and BB05, subsurface reactive Fe availability is limited by consumption via surficial pyrite genesis. Here, pyrite formation is mostly terminated by ~80 cmbsf, leaving the ^{32}S-enriched signal inherited from early-formed pyrite to dominate the bulk signal, even at depth (Fig. 2; Liu et al., 2020a).

Interestingly, the $\delta^{34}S$ of pore fluid aqueous H_2S decreases below the sulfate–methane transition (SMT) at site BB03 (Fig. 3A). This unexpected inflection within the sulfate-depleted methanogenic zone (Fig. S4) likely signals the operation of a cryptic, Fe-driven, sulfur cycle beneath the SMT (Holmkvist et al., 2011; Liu et al., 2020b). The H_2S gradient beneath the SMT (Fig. S1B) drives a downward diffusion of ^{34}S-enriched H_2S, which is partially oxidized by deeply buried Fe-oxides. Manifest as a decrease in H_2S-$\delta^{34}S$ (Fig. 3A), the production of sulfur

intermediates fuels successive disproportionation, generating ^{34}S-depleted H_2S and ^{34}S-enriched SO_4^{2-} (Canfield and Thamdrup, 1994). Unfortunately, the concentration of sulfate is maintained around a background of 10 µM via microbial consumption (Pellerin et al., 2018), which provides an analytical hurdle that prevents us from tracing the expected ^{34}S enrichment within the sulfate pool. A similar $\delta^{34}S$ profile of H_2S might be expected in other marine sediments where reactive Fe-oxides are abundant below the SMT.

PYRITE FORMATION UNDER NON-STEADY-STATE CONDITIONS

Besides sediment-hosted diagenetic processes, pyrite formation is influenced by bottom-water chemistry. Accordingly, the abundance of early-formed pyrite formed near the sediment–water interface (i.e., in the upper 10 cm) may have varied over time. Using a two end-member mixing model (see Supplemental Material) the sediments between 50–200 cmbsf were found to have much lower contents of early-formed pyrite compared with those found in the upper 50 cm of core BB03 (Fig. 4A). Furthermore, the downcore profile of pyrite-$\delta^{34}S$ values can be broadly reproduced by changing initial, near-surface pyrite formation (Fig. 4B–C), confirming that sediments possessing less early-formed pyrite were able to evolve higher pyrite-$\delta^{34}S$ values through the enhanced addition of pyrite at depth because the reactive Fe delivered to the sediment–water interface wasn't depleted through shallow pyrite formation.

Contemporary deoxygenation of the Baltic Sea is the most likely explanation for the decreased contents of early-formed pyrite seen during the earlier Holocene relative to the present-day. Although the Bornholm Basin is currently bathed by hypoxic waters with seasonal development of anoxia, the area and severity of hypoxia have undergone a ten-fold expansion over the past 115 years, fueled by heightened eutrophication and global warming (Carstensen et al.,

2014). Prior to these anthropogenic changes, pre-industrial bottom-waters were likely to have been more oxygenated, limiting pyrite formation via more intense bioturbation and heightened re-oxidation of reduced sulfur at the sediment–water interface (Jørgensen and Nelson, 2004). The bioturbation intensity determined using the ichnofabric index indeed varied significantly between "bioturbation absent" and "moderate bioturbation" throughout a 10-meter-deep core with weak or absent lamination at the same site (Andrén et al., 2015). Likewise, changes in bioturbation intensity are expected to impact the subsurface pyrite-$\delta^{34}S$ in other marine settings (cf. Fike et al., 2015).

Interestingly, such variation in the early-formed pyrite content is not ubiquitous and is not observed at site BB02 (Liu et al., 2020a), suggesting that bottom-water oxygen availability was more spatially variable in the past. Although both sites BB02 (96 m) and BB03 (84 m) reside below the current halocline (50–80 m), where dissolved oxygen is scarce, the Bornholm Basin was most likely more weakly stratified in the past, with enhanced vertical mixing and a deeper halocline (Carstensen et al., 2014; Väli et al., 2013). Consequently, site BB03 would have been more frequently bathed by oxygenated bottom-waters before the recent expansion of hypoxia, limiting pyrite formation near the sediment surface. The deepest basin, however, would have remained hypoxic with transient oxygenation events, sustaining early pyrite formation at site BB02 throughout much of the Holocene. Since coastal hypoxia is a worsening problem observed worldwide (e.g., Middelburg and Levin, 2009), we anticipate that a similar pyrite-$\delta^{34}S$ response to bottom-water deoxygenation may begin to be recognized on a much greater spatial scale.

CONCLUSIONS

Local oxygen availability and sedimentation rate combine to regulate near-surface pyritization and the availability of reactive Fe at depth. A greater survival rate (i.e., enhanced burial)

of reactive Fe, in turn, sustains sediment-hosted pyrite genesis, driving bulk pyrite $\delta^{34}S$ values more positive via the subsurface addition of ^{34}S-enriched pyrite. Although geological $\delta^{34}S$ records of pyrite are widely used to reconstruct global changes in C-S-Fe cycling, the large spatial differences identified in our pyrite-$\delta^{34}S$ records, spanning some 10 km within the Bornholm Basin, demonstrate that the $\delta^{34}S$ signal is heavily influenced by the prevailing localized geochemical and depositional conditions. Such a diagenetic influence is not expected to be constrained to Baltic post-glacial successions, but is anticipated to be relevant to dynamic settings that feature non-steady-state sedimentation. Consistent with this prediction, the ever-growing $\delta^{34}S$ database has revealed significant heterogeneities in supposedly time-equivalent modern and ancient pyrite-$\delta^{34}S$ records alike (e.g., Hammarlund et al., 2012). In light of our findings, this variability can be readily explained by site-specific depositional and diagenetic processes. While serving as a note of caution, these findings expose $\delta^{34}S$ systematics as a valuable proxy capable of decoding localized sedimentological and environmental changes throughout Earth history.

ACKNOWLEDGMENTS

We acknowledge the skipper and crew of R/V *Aurora*, and colleagues at the Center for Geomicrobiology for assistance during sampling. We recognize contributions and technical assistance from Susann Henkel, Ingrid Stimac, Karina Bomholt Oest, Jeanette Pedersen and Felix Beulig. This work was supported by the Danish National Research Foundation (DNRF grant #104), the Danish Council for Independent Research (DFF–7014-00196), the European Research Council (ERC Advanced Grant #294200), the Helmholtz Association (Alfred Wegener Institute Helmholtz Centre for Polar and Marine Research in Bremerhaven), and the Alfred P. Sloan Foundation via the Deep Carbon Observatory. GA acknowledges financial support from the Israel Science Foundation (2361/19). AP is supported by the Zuckerman STEM Leadership Program. GI recognizes a MISTI award ("Decrypting Early Earth's Oxygenation") in addition to continued support from R. Summons under the auspices of the Simons Collaboration on the Origin of Life. AJF acknowledges a Marie-Curie European Fellowship (SedSulphOx, MSCA 746872). AVT acknowledges financial support from the National Environmental Research Council (NERC–NE/T006838/1).

REFERENCES CITED

Andrén, T., Jørgensen, B. B., et al., 2015, Proceedings of the Integrated Ocean Drilling Program, Site M0065, Volume 347: College Station, Texas, Integrated Ocean Drilling Program, CD-ROM.

Berner, R. A., 1984, Sedimentary pyrite formation: An update: Geochimica et Cosmochimica Acta, v. 48, no. 4, p. 605-615, doi:10.1016/0016-7037(84)90089-9.

Butler, I. B., Böttcher, M. E., Rickard, D., and Oldroyd, A., 2004, Sulfur isotope partitioning during experimental formation of pyrite via the polysulfide and hydrogen sulfide pathways: implications for the interpretation of sedimentary and hydrothermal pyrite isotope records: Earth and Planetary Science Letters, v. 228, no. 3, p. 495-509, doi:10.1016/j.epsl.2004.10.005.

Canfield, D., and Thamdrup, B., 1994, The production of ^{34}S-depleted sulfide during bacterial disproportionation of elemental sulfur: Science, v. 266, no. 5193, p. 1973-1975, doi:10.1126/science.11540246.

Canfield, D. E., 2001, Biogeochemistry of Sulfur Isotopes: Reviews in Mineralogy and Geochemistry, v. 43, no. 1, p. 607-636, doi:10.2138/gsrmg.43.1.607.

Canfield, D. E., and Teske, A., 1996, Late Proterozoic rise in atmospheric oxygen concentration inferred from phylogenetic and sulphur-isotope studies: Nature, v. 382, no. 6587, p. 127-132, doi:10.1038/382127a0.

Carstensen, J., Andersen, J. H., Gustafsson, B. G., and Conley, D. J., 2014, Deoxygenation of the Baltic Sea during the last century: Proceedings of the National Academy of Sciences, v. 111, no. 15, p. 5628-5633, doi:10.1073/pnas.1323156111.

Chernyavsky, B. M., and Wortmann, U. G., 2007, REMAP: A reaction transport model for isotope ratio calculations in porous media: Geochemistry, Geophysics, Geosystems, v. 8, no. 2, doi:10.1029/2006gc001442.

Fike, D. A., Bradley, A. S., and Rose, C. V., 2015, Rethinking the ancient sulfur cycle: Annual Review of Earth and Planetary Sciences, v. 43, no. 1, p. 593-622, doi:10.1146/annurev-earth-060313-054802.

Garrels, R. M., and Lerman, A., 1981, Phanerozoic cycles of sedimentary carbon and sulfur: Proceedings of the National Academy of Sciences, v. 78, no. 8, p. 4652-4656, doi:10.1073/pnas.78.8.4652.

Gill, B. C., Lyons, T. W., Young, S. A., Kump, L. R., Knoll, A. H., and Saltzman, M. R., 2011, Geochemical evidence for widespread euxinia in the Later Cambrian ocean: Nature, v. 469, no. 7328, p. 80-83, doi:10.1038/nature09700.

Goldhaber, M. B., and Kaplan, I. R., 1975, Controls and consequences of sulfate reduction rates in recent marine sediments: Soil Science, v. 119, no. 1, p. 42-55.

Hammarlund, E. U., Dahl, T. W., Harper, D. A. T., Bond, D. P. G., Nielsen, A. T., Bjerrum, C. J., Schovsbo, N. H., Schönlaub, H. P., Zalasiewicz, J. A., and Canfield, D. E., 2012, A sulfidic driver for the end-Ordovician mass extinction: Earth and Planetary Science Letters, v. 331-332, p. 128-139, doi:10.1016/j.epsl.2012.02.024.

Hilligsøe, K. M., Jensen, J. B., Ferdelman, T. G., Fossing, H., Lapham, L., Røy, H., and Jørgensen, B. B., 2018, Methane fluxes in marine sediments quantified through core analyses and seismo-acoustic mapping (Bornholm Basin, Baltic Sea): Geochimica et Cosmochimica Acta, v. 239, p. 255-274, doi:10.1016/j.gca.2018.07.040.

Holmkvist, L., Ferdelman, T. G., and Jørgensen, B. B., 2011, A cryptic sulfur cycle driven by iron in the methane zone of marine sediment (Aarhus Bay, Denmark): Geochimica et Cosmochimica Acta, v. 75, no. 12, p. 3581-3599, doi:10.1016/j.gca.2011.03.033.

Jørgensen, B. B., 1979, A theoretical model of the stable sulfur isotope distribution in marine sediments: Geochimica et Cosmochimica Acta, v. 43, no. 3, p. 363-374, doi:10.1016/0016-7037(79)90201-1.

Jørgensen, B. B., Findlay, A. J., and Pellerin, A., 2019, The biogeochemical sulfur cycle of marine sediments: Frontiers in Microbiology, v. 10:849, doi:10.3389/fmicb.2019.00849.

Jørgensen, B. B., and Nelson, D. C., 2004, Sulfide oxidation in marine sediments: Geochemistry meets microbiology, *in* Amend, J. P., Edwards, K. J., and Lyons, T. W., eds., Sulfur Biogeochemistry - Past and Present, Geological Society of America, p. 63-82.

Lang, X., Tang, W., Ma, H., and Shen, B., 2020, Local environmental variation obscures the interpretation of pyrite sulfur isotope records: Earth and Planetary Science Letters, v. 533, p. 116056, doi:10.1016/j.epsl.2019.116056.

Liu, J., Pellerin, A., Antler, G., Kasten, S., Findlay, A. J., Dohrmann, I., Røy, H., Turchyn, A. V., and Jørgensen, B. B., 2020a, Early diagenesis of iron and sulfur in Bornholm Basin sediments: The role of near-surface pyrite formation: Geochimica et Cosmochimica Acta, v. 284, p. 43-60, doi:10.1016/j.gca.2020.06.003.

Liu, J., Pellerin, A., Izon, G., Wang, J., Antler, G., Liang, J., Su, P., Jørgensen, B. B., and Ono, S., 2020b, The multiple sulphur isotope fingerprint of a sub-seafloor oxidative sulphur cycle driven by iron: Earth and Planetary Science Letters, v. 536, p. 116165, doi:10.1016/j.epsl.2020.116165.

Liu, X., Fike, D., Li, A., Dong, J., Xu, F., Zhuang, G., Rendle-Bühring, R., and Wan, S., 2019, Pyrite sulfur isotopes constrained by sedimentation rates: Evidence from sediments on the East China Sea inner shelf since the late Pleistocene: Chemical Geology, v. 505, p. 66-75, doi:10.1016/j.chemgeo.2018.12.014.

März, C., Hoffmann, J., Bleil, U., De Lange, G., and Kasten, S., 2008, Diagenetic changes of magnetic and geochemical signals by anaerobic methane oxidation in sediments of the Zambezi deep-sea fan (SW Indian Ocean): Marine Geology, v. 255, no. 3, p. 118-130, doi:10.1016/j.margeo.2008.05.013.

Masterson, A. L., 2016, Multiple Sulfur Isotope Applications in Diagenetic Models and Geochemical Proxy Records [Doctoral Dissertation]: Harvard University, 159 p.

Middelburg, J. J., and Levin, L. A., 2009, Coastal hypoxia and sediment biogeochemistry: Biogeosciences, v. 6, no. 7, p. 1273-1293, doi:10.5194/bg-6-1273-2009.

Ono, S., Wing, B., Johnston, D., Farquhar, J., and Rumble, D., 2006, Mass-dependent fractionation of quadruple stable sulfur isotope system as a new tracer of sulfur biogeochemical cycles: Geochimica et Cosmochimica Acta, v. 70, no. 9, p. 2238-2252, doi:10.1016/j.gca.2006.01.022.

Pasquier, V., Sansjofre, P., Rabineau, M., Revillon, S., Houghton, J., and Fike, D. A., 2017, Pyrite sulfur isotopes reveal glacial−interglacial environmental changes: Proceedings of the National Academy of Sciences, v. 114, no. 23, p. 5941-5945, doi:10.1073/pnas.1618245114.

Pellerin, A., Antler, G., Røy, H., Findlay, A., Beulig, F., Scholze, C., Turchyn, A. V., and Jørgensen, B. B., 2018, The sulfur cycle below the sulfate-methane transition of marine

290 sediments: Geochimica et Cosmochimica Acta, v. 239, p. 74-89,
291 doi:10.1016/j.gca.2018.07.027.
292 Rickard, D., and Luther, G. W., 2007, Chemistry of Iron Sulfides: Chemical Reviews, v. 107, no.
293 2, p. 514-562, doi:10.1021/cr0503658.
294 Riedinger, N., Brunner, B., Krastel, S., Arnold, G. L., Wehrmann, L. M., Formolo, M. J., Beck,
295 A., Bates, S. M., Henkel, S., and Kasten, S., 2017, Sulfur cycling in an iron oxide-
296 dominated, dynamic marine depositional system: The Argentine continental margin:
297 Frontiers in Earth Science, v. 5:33, doi:10.3389/feart.2017.00033.
298 Riedinger, N., Pfeifer, K., Kasten, S., Garming, J. F. L., Vogt, C., and Hensen, C., 2005,
299 Diagenetic alteration of magnetic signals by anaerobic oxidation of methane related to a
300 change in sedimentation rate: Geochimica et Cosmochimica Acta, v. 69, no. 16, p. 4117-
301 4126, doi:10.1016/j.gca.2005.02.004.
302 Shawar, L., Halevy, I., Said-Ahmad, W., Feinstein, S., Boyko, V., Kamyshny, A., and Amrani,
303 A., 2018, Dynamics of pyrite formation and organic matter sulfurization in organic-rich
304 carbonate sediments: Geochimica et Cosmochimica Acta, v. 241, p. 219-239,
305 doi:10.1016/j.gca.2018.08.048.
306 Sim, M. S., Bosak, T., and Ono, S., 2011, Large Sulfur Isotope Fractionation Does Not Require
307 Disproportionation: Science, v. 333, no. 6038, p. 74-77, doi:10.1126/science.1205103.
308 Väli, G., Meier, H. E. M., and Elken, J., 2013, Simulated halocline variability in the Baltic Sea
309 and its impact on hypoxia during 1961–2007: Journal of Geophysical Research: Oceans,
310 v. 118, no. 12, p. 6982-7000, doi:10.1002/2013JC009192.
311 Wijsman, J. W. M., Middelburg, J. J., Herman, P. M. J., Böttcher, M. E., and Heip, C. H. R.,
312 2001, Sulfur and iron speciation in surface sediments along the northwestern margin of

the Black Sea: Marine Chemistry, v. 74, no. 4, p. 261-278, doi:10.1016/S0304-4203(01)00019-6.

315 FIGURES

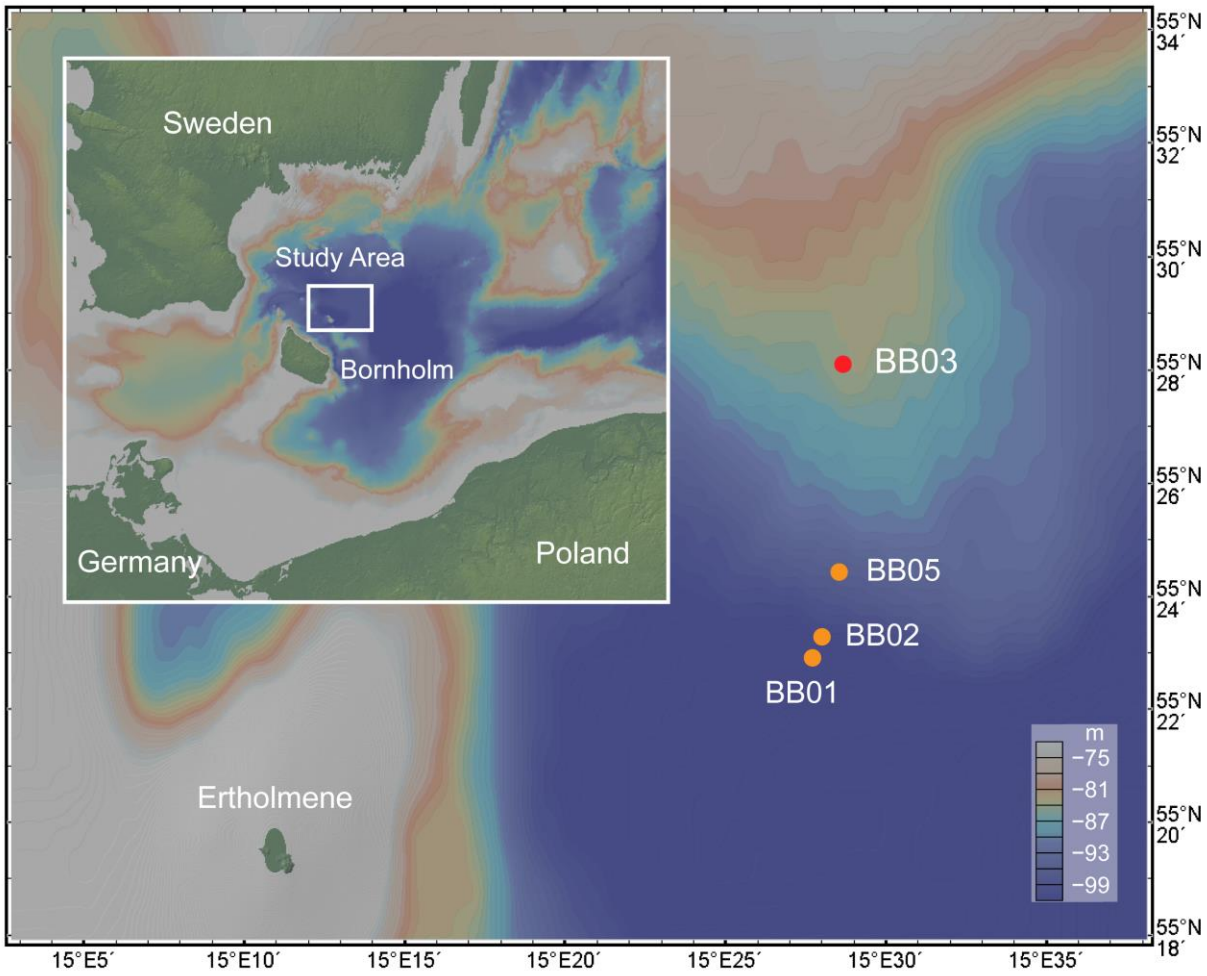

316

317 Figure 1. Bathymetric maps locating site BB03 and its neighboring sites within the Bornholm
318 Basin contextualized within the wider Southwestern Baltic Sea (insert). Maps were generated via
319 GeoMapApp.

320

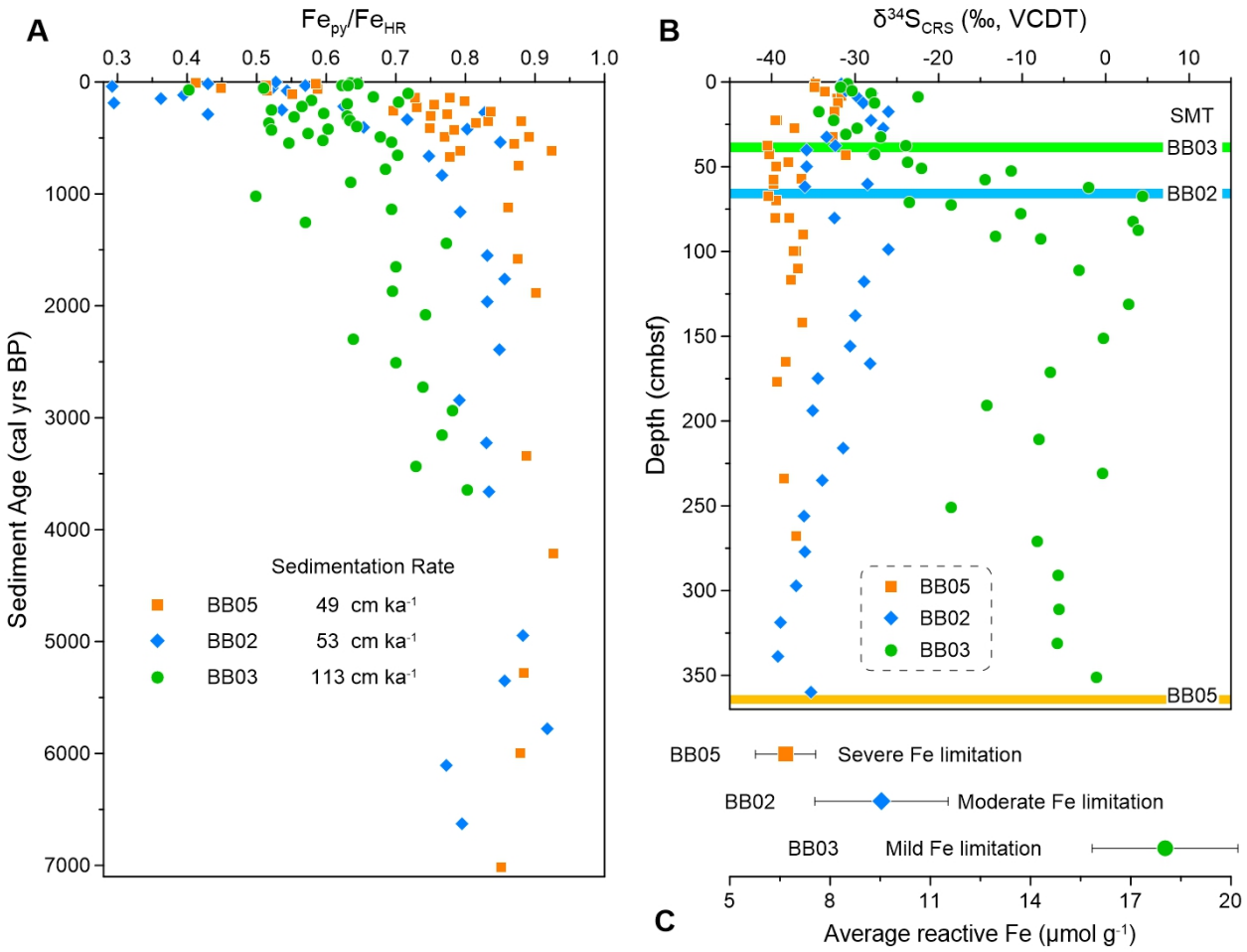

321

322 Figure 2. Comparison of geochemical data for sites BB05, BB02 and BB03. (A) The extent of
323 pyritization (Fe_{py}/Fe_{HR}). (B) The $\delta^{34}S$ of chromium reducible sulfur (CRS, predominantly pyrite).
324 (C) The average reactive iron contents (± 1σ) of Holocene-aged sediments in the Bornholm Basin.
325 The horizontal bars in (B) show the depth of the SMT. The raw data in (C) are shown in Fig. 3C.
326 Data from cores BB02 and BB05 are from Liu et al. (2020a).

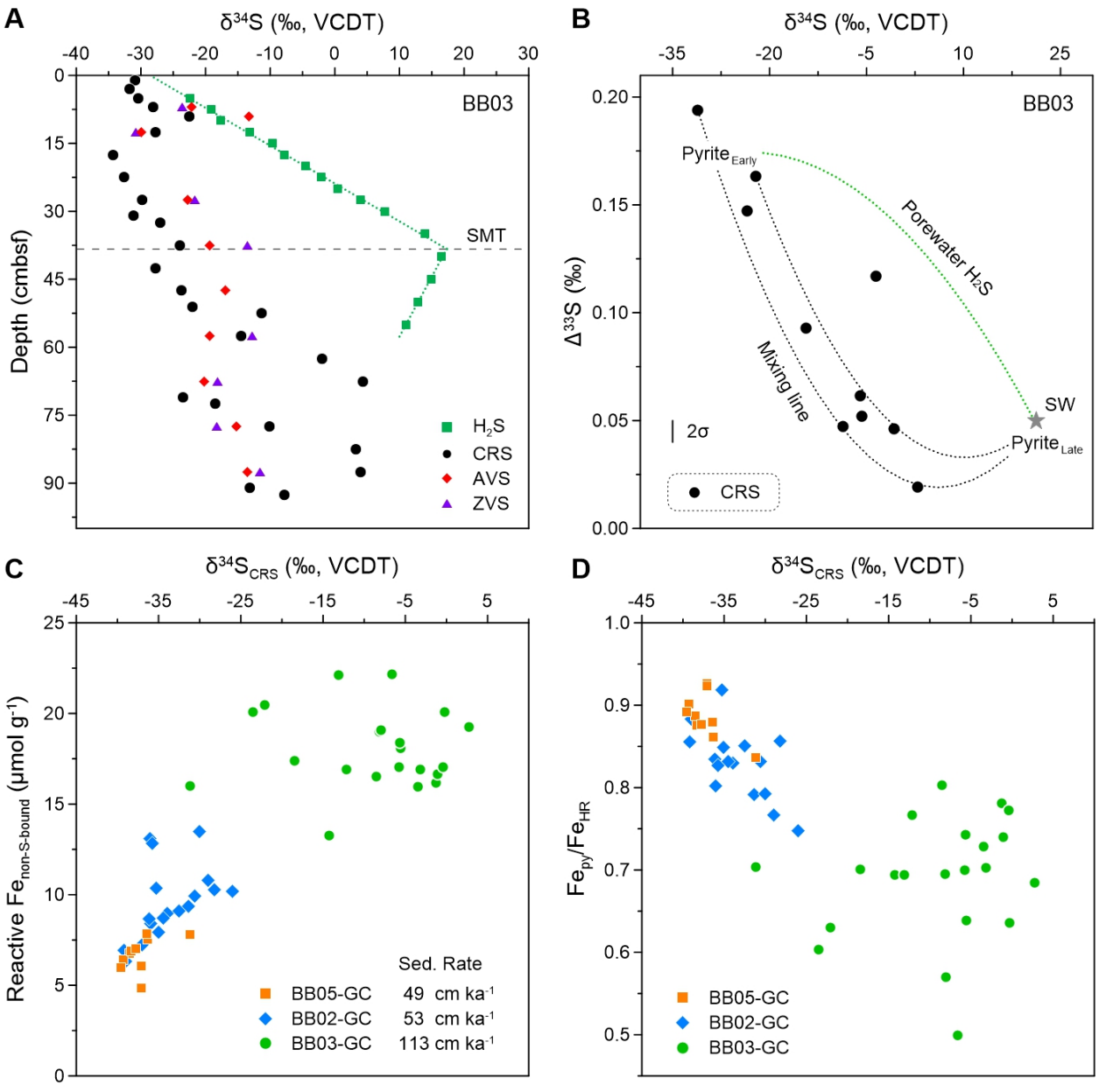

Figure 3. Sulfur and iron geochemistry from the Bornholm Basin. (A) Fraction-specific $\delta^{34}S$ values from the upper 100 cm of site BB03. (B) CRS-derived multiple sulfur isotope data from site BB03. (C–D) Reactive iron content (C) and reactive-iron-normalized pyrite content (Fe_{py}/Fe_{HR}; D) versus CRS-derived $\delta^{34}S$ values from sites BB05, BB02 and BB03. The green and black dotted curves in (B) depict the trajectory of H_2S (cf. Masterson, 2016) and the mixing line, respectively. The end-

members defining the mixing lines are based on measured and literature data (cf. Liu et al. 2020b). Data from cores BB02 and BB05 are from Liu et al. (2020a).

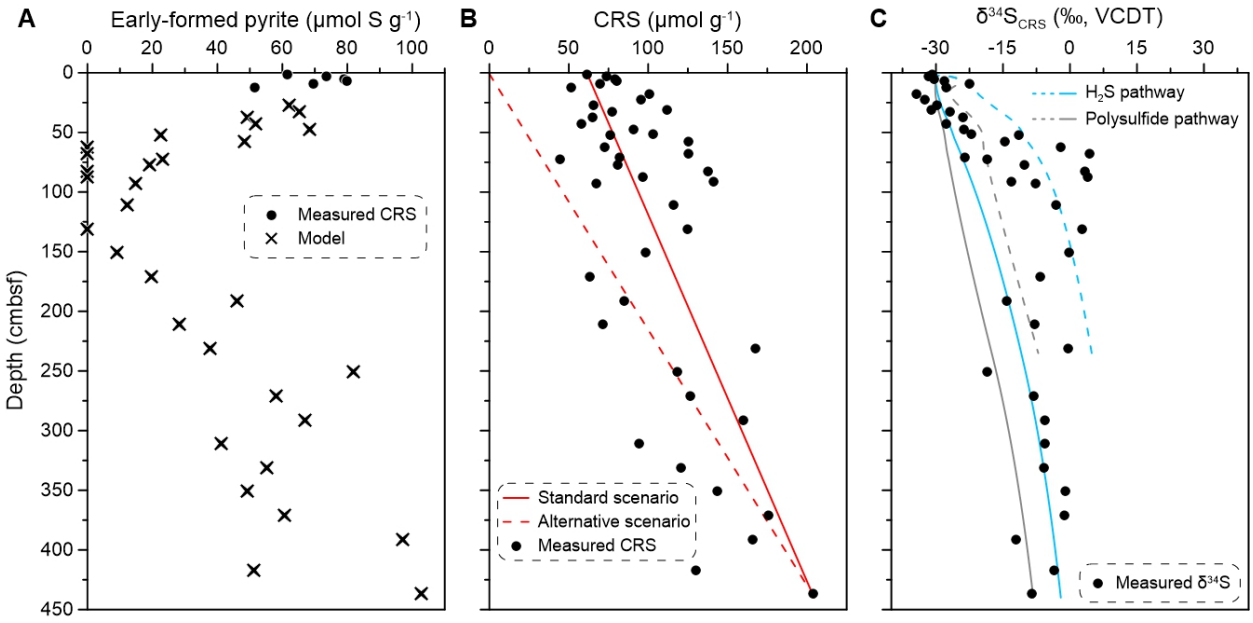

Figure 4. CRS data and model outputs describing pyrite growth at site BB03. (A) Early-formed pyrite contents. The measured CRS contents in the upper 10 cm are shown for comparison. (B) Measured CRS content and the variable rates of pyrite formation used within the model. (C) Downcore measured and modeled $\delta^{34}S_{CRS}$. The solid lines describe high pyrite formation at the sediment–water interface (standard scenario), while the dashed lines depict an alternative scenario where pyrite formation starts only below the sediment–water interface.

[1]GSA Data Repository item 20XXxxx, supplemental methods, diagenetic model, Table S1 and Figures S1–5, is available online at www.geosociety.org/pubs/ft20XX.htm, or on request from editing@geosociety.org.